Int. J. Electrochem. Sci., 15 **(2020)** 304 – 310, doi: 10.20964/2020.01.44

International Journal of
ELECTROCHEMICAL
SCIENCE
www.electrochemsci.org

Short Communication

Novel Composite Electrolyte of Double-Doped Ceria-Sulphate for Medium Temperature Fuel Cells

Wenbao Zhang, Tianhui Hu, Ruijuan Shi[*,*], Hongtao Wang* [*]

Anhui Provincial Key Laboratory for Degradation and Monitoring of Pollution of the Environment; School of Chemical and Material Engineering, Fuyang Normal University, Fuyang 236037, China
[*]E-mail: hwang@fynu.edu.cn; rjshi@fynu.edu.cn

Received: 9 September 2019 / *Accepted:* 15 October 2019 / *Published:* 30 November 2019

In this study, Gd^{3+} and Er^{3+} double-doped CeO_2 was synthesized by a microemulsion method. $Ce_{0.8}Er_{0.1}Gd_{0.1}O_{2-\alpha}$-$K_2SO_4$-$Li_2SO_4$ composite electrolyte was prepared by mixing $Ce_{0.8}Er_{0.1}Gd_{0.1}O_{2-\alpha}$ powder with binary sulphates. The structures of $Ce_{0.8}Er_{0.1}Gd_{0.1}O_{2-\alpha}$ and $Ce_{0.8}Er_{0.1}Gd_{0.1}O_{2-\alpha}$-$K_2SO_4$-$Li_2SO_4$ were characterized by X-ray diffraction (XRD) and Raman spectrometer. XRD spectra showed that the $Ce_{0.8}Er_{0.1}Gd_{0.1}O_{2-\alpha}$ structure was not affected by K_2SO_4-Li_2SO_4. Raman spectrometer further indicated that the prepared $Ce_{0.8}Er_{0.1}Gd_{0.1}O_{2-\alpha}$-$K_2SO_4$-$Li_2SO_4$ had a cubic structure of CeO_2 and the existence of SO_4^{2-}. The maximum conductivity of $Ce_{0.8}Er_{0.1}Gd_{0.1}O_{2-\alpha}$-$K_2SO_4$-$Li_2SO_4$ reached 0.21 $S \cdot cm^{-1}$ at 700 °C.

Keywords: Defects; Composite; Electrolytes; Hydrogen; Fuel cell; Conductivity

1. INTRODUCTION

Fuel cells can directly convert chemical energy into electrical energy without burning. To make yttria-stabilized zirconia (YSZ) achieve sufficient ionic conductivity, traditional solid oxide fuel cells (SOFCs) are usually operated at 800–1000 °C. Reducing operating temperature can effectively improve the two major problems of high temperature operation: short life and unreliability [1-16].

Electrolyte is the core component of SOFCs. Doped ceria is the electrolyte material which has the highest ionic conductivity in the intermediate temperature range (400–700 °C) [17-20]. Colet-Lagrille et al. synthesized $Mo_xCe_{1-x}O_{2-\delta}$ using a combustion method and $Mo_{0.1}Ce_{1.9}O_{2-\delta}$ had the maximum conductivities of 1.87×10^{-3} $S \cdot cm^{-1}$ and 9.37×10^{-1} $S \cdot cm^{-1}$ in air and H_2 at 800 °C [19]. However, part of Ce^{4+} being reduced to Ce^{3+} in reducing atmosphere is the biggest problem of doped ceria. Co-doping is a very effective means of inhibiting reduction of Ce^{4+}. Double doped ceria usually

has lower activation energies than single doped ceria [21-26]. Parkash et al. found that $Ce_{0.8}Nd_{0.18}Y_{0.02}O_{1.9}$ had higher conductivities than that of $Ce_{0.8}Nd_{0.2}O_{1.9}$ [23].

In addition, composite electrolytes can also increase ionic conductivity and effectively inhibit the electronic conduction of Ce^{4+} [27-35]. Park et al. found that barium zirconate-ceria composite electrolyte had higher conductivities than that of single $BaZr_{0.85}Y_{0.15}O_{3-\delta}$ [27]. Marques et al. investigated ceria-carbonate composite electrolytes which had long-term stability in air, CO_2 and H_2-N_2 atmospheres [28]. Ceria-carbonate composite electrolytes had high ionic conductivities at medium temperature, therefore, high output fuel cell performances could be obtained without a film forming. As far as we know, there are few reports about ceria-sulphate composite electrolytes.

In this study, Gd^{3+} and Er^{3+} double-doped CeO_2 was synthesized by a microemulsion method. $Ce_{0.8}Er_{0.1}Gd_{0.1}O_{2-\alpha}$-$K_2SO_4$-$Li_2SO_4$ composite electrolyte was prepared by mixing $Ce_{0.8}Er_{0.1}Gd_{0.1}O_{2-\alpha}$ powder with binary sulphates. The single and composite electrolytes were characterized and studied in terms of phase, morphology, conductivity and fuel cell performances at 400–700 °C.

2. EXPERIMENTAL

$Ce_{0.8}Er_{0.1}Gd_{0.1}O_{2-\alpha}$ electrolyte was prepared by the microemulsion method. Er_2O_3, Gd_2O_3 and $(NH_4)_2Ce(NO_3)_6$ with mole ratios of 1:1:8 were dissolved and mixed evenly. Anhydrous alcohol, PEG and cyclohexane were added to form the microemulsion A according to the total molar number of metal cations in the solution. PEG, $(NH_4)_2CO_3$, NH_4OH, anhydrous alcohol and cyclohexane were mixed evenly and dripped into microemulsion A with continuous stirring. After being filtrated and dried for 2 h, the nanoparticles were obtained. The nanoparticles were calcined at 900 °C and 1500 °C for 5 h, to get $Ce_{0.8}Er_{0.1}Gd_{0.1}O_{2-\alpha}$. In the prepared $Ce_{0.8}Er_{0.1}Gd_{0.1}O_{2-\alpha}$ powder, K_2SO_4 and Li_2SO_4 (1:1 mole ratio) with the required proportions were added [36]. $Ce_{0.8}Er_{0.1}Gd_{0.1}O_{2-\alpha}$-$K_2SO_4$-$Li_2SO_4$ composite electrolyte was prepared by heating the mixture for 1 h at 750 °C.

The structures of $Ce_{0.8}Er_{0.1}Gd_{0.1}O_{2-\alpha}$ and $Ce_{0.8}Er_{0.1}Gd_{0.1}O_{2-\alpha}$-$K_2SO_4$-$Li_2SO_4$ were characterized by X-ray diffraction and Raman spectrometer. The $Ce_{0.8}Er_{0.1}Gd_{0.1}O_{2-\alpha}$ and $Ce_{0.8}Er_{0.1}Gd_{0.1}O_{2-\alpha}$-$K_2SO_4$-$Li_2SO_4$ were polished with sandpaper and coated with Pd-Ag slurry on both sides. The samples were dried and placed in an electric furnace. The AC impedance spectra of the samples were measured in air at 400-700 °C by electrochemical workstation. The test frequency ranged from 1 to 10^5 Hz and the signal voltage was 0.05 V. The assembled fuel cells of $Ce_{0.8}Er_{0.1}Gd_{0.1}O_{2-\alpha}$ and $Ce_{0.8}Er_{0.1}Gd_{0.1}O_{2-\alpha}$-$K_2SO_4$-$Li_2SO_4$ were placed in hydrogen and oxygen atmospheres, respectively. The volt-ampere curves and impedance of fuel cells under open circuit state were measured by electrochemical workstation at 700 °C.

3. RESULTS AND DISCUSSION

Fig. 1 is a comparison of XRD spectra of $Ce_{0.8}Er_{0.1}Gd_{0.1}O_{2-\alpha}$ and $Ce_{0.8}Er_{0.1}Gd_{0.1}O_{2-\alpha}$- K_2SO_4-Li_2SO_4 prepared at different calcination temperatures. From Fig. 1, it can be seen that the diffraction

peaks of all samples are sharp, which indicates that the crystallinity is good. The half-peak width of the 900 °C calcined sample is wider, which indicates that the crystal sizes are smaller. After the samples are sintered at 1500 °C for 5 h, the peak strength increases and the half-peak width narrows obviously, which indicate that the crystal sizes increase. In addition to CeO_2 phase, a small amount of $KLiSO_4$ phase exists in the $Ce_{0.8}Er_{0.1}Gd_{0.1}O_{2-\alpha}$-$K_2SO_4$-$Li_2SO_4$ sample. Maybe this is because K_2SO_4-Li_2SO_4 is molten while being heated at 750 °C for 1 h. While $Ce_{0.8}Er_{0.1}Gd_{0.1}O_{2-\alpha}$-$K_2SO_4$-$Li_2SO_4$ is cooled to room temperature, most of K_2SO_4-Li_2SO_4 does not crystallize and exists in an amorphous form. Therefore, $KLiSO_4$ has only weak peaks in the XRD pattern. XRD spectra show that the $Ce_{0.8}Er_{0.1}Gd_{0.1}O_{2-\alpha}$ structure is not affected by K_2SO_4-Li_2SO_4, which means that it has good corrosion resistance to molten sulphates [21-28].

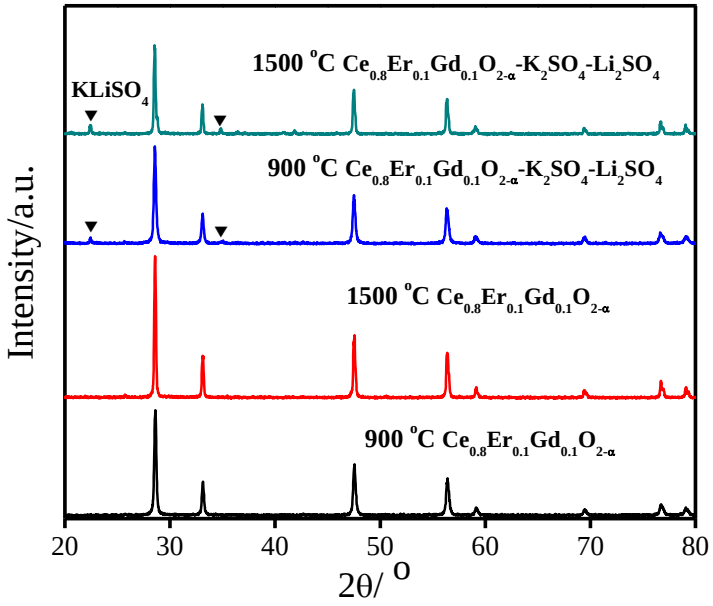

Figure 1. XRD spectra of $Ce_{0.8}Er_{0.1}Gd_{0.1}O_{2-\alpha}$ (900 °C, 1500 °C) and $Ce_{0.8}Er_{0.1}Gd_{0.1}O_{2-\alpha}$- K_2SO_4-Li_2SO_4 (900 °C, 1500 °C).

Raman spectra of $Ce_{0.8}Er_{0.1}Gd_{0.1}O_{2-\alpha}$ (900 °C, 1500 °C) and $Ce_{0.8}Er_{0.1}Gd_{0.1}O_{2-\alpha}$-$K_2SO_4$-$Li_2SO_4$ (1500 °C) are shown in Fig. 2. There are strong Raman activity peaks in the F_{2g} mode of Ce-O-Ce symmetrical stretching vibration for $Ce_{0.8}Er_{0.1}Gd_{0.1}O_{2-\alpha}$ (1500 °C) and $Ce_{0.8}Er_{0.1}Gd_{0.1}O_{2-\alpha}$- K_2SO_4-Li_2SO_4 (1500 °C) at 497 and 520 cm^{-1}. Compared with the 1500 °C sintered samples, 900 °C sintered $Ce_{0.8}Er_{0.1}Gd_{0.1}O_{2-\alpha}$ has imperfect Raman peaks because of its small particle size. Although $Ce_{0.8}Er_{0.1}Gd_{0.1}O_{2-\alpha}$ (900 °C) structure agrees with the CeO_2 in Fig. 1, the grain boundary is not formed well in Fig. 2. O_h vibrational mode corresponds to 674 cm^{-1}. Raman peaks around 556 cm^{-1} correspond to the S-O bending deformation vibration. Raman peaks near 980 cm^{-1} are attributed to the S-O symmetrical telescopic vibration [37-39]. This shows that the prepared $Ce_{0.8}Er_{0.1}Gd_{0.1}O_{2-\alpha}$-$K_2SO_4$-$Li_2SO_4$ has a cubic structure of CeO_2 and the existence of SO_4^{2-}, which is consistent with Fig. 1.

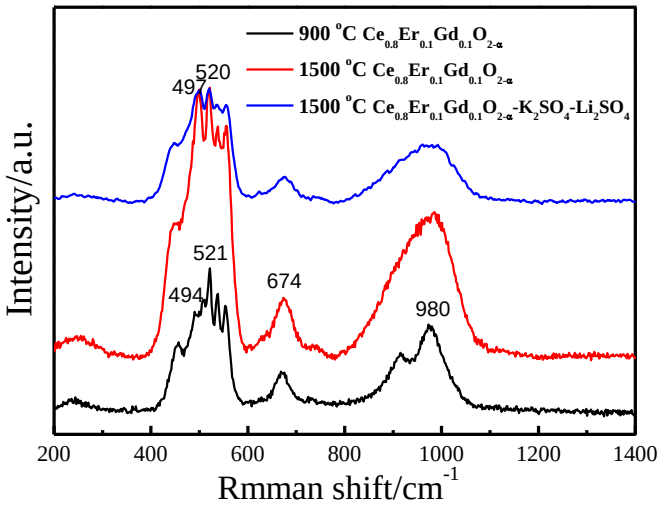

Figure 2. Raman spectra of $Ce_{0.8}Er_{0.1}Gd_{0.1}O_{2-\alpha}$ (900 °C, 1500 °C) and $Ce_{0.8}Er_{0.1}Gd_{0.1}O_{2-\alpha}$- K_2SO_4-Li_2SO_4 (1500 °C).

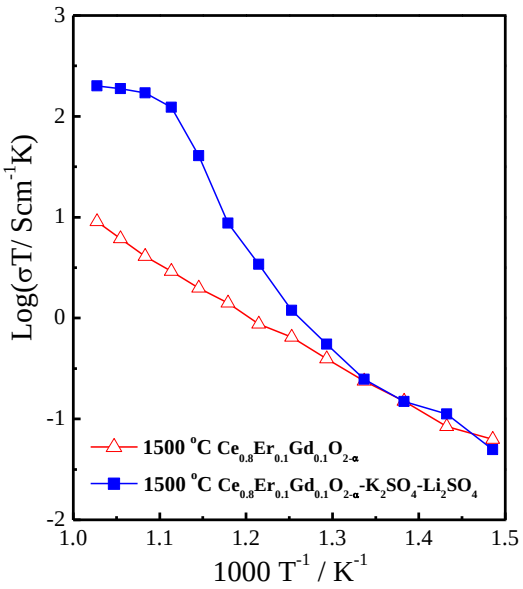

Figure 3. Arrhenius curves of $Ce_{0.8}Er_{0.1}Gd_{0.1}O_{2-\alpha}$ (1500 °C) and $Ce_{0.8}Er_{0.1}Gd_{0.1}O_{2-\alpha}$-$K_2SO_4$-$Li_2SO_4$ (1500 °C) at 400-700 °C.

Fig. 3 shows Arrhenius curves of $Ce_{0.8}Er_{0.1}Gd_{0.1}O_{2-\alpha}$ (1500 °C) and $Ce_{0.8}Er_{0.1}Gd_{0.1}O_{2-\alpha}$- K_2SO_4-Li_2SO_4 (1500 °C) in air at 400-700 °C. The ionic conduction of $Ce_{0.8}Er_{0.1}Gd_{0.1}O_{2-\alpha}$ (1500 °C) could be ascribed to the partial substitution of Ce^{4+} with Er^{3+} and Gd^{3+} ions which formed oxygen vacancies [18-23]. The Arrhenius curve of $Ce_{0.8}Er_{0.1}Gd_{0.1}O_{2-\alpha}$-$K_2SO_4$-$Li_2SO_4$ has a turning point where the conductivity transits near the temperature of 625 °C. This may be attributed to the change of the concentration of charge carriers. The enhancement effect of conductivity is caused by the interface between $Ce_{0.8}Er_{0.1}Gd_{0.1}O_{2-\alpha}$ and K_2SO_4-Li_2SO_4 [32–35]. Below the transition temperature, sulphate is solid phase, which hinders ionic charge carriers' jump and mobility. Ions are mainly transported through the interface and bulk of $Ce_{0.8}Er_{0.1}Gd_{0.1}O_{2-\alpha}$. Therefore, the conductivities of the composite are

equivalent to $Ce_{0.8}Er_{0.1}Gd_{0.1}O_{2-\alpha}$. With the increase of temperature, the melting process of sulphate begins to extend from the interface region to bulk phase. Above the transition temperature, the sulphate in the interface region begins to melt, which is conducive to the conduction of ion defects through the interface region. The maximum conductivity of $Ce_{0.8}Er_{0.1}Gd_{0.1}O_{2-\alpha}$-$K_2SO_4$-$Li_2SO_4$ reached 2.1×10^{-1} $S\cdot cm^{-1}$ at 700 °C [23, 32-35].

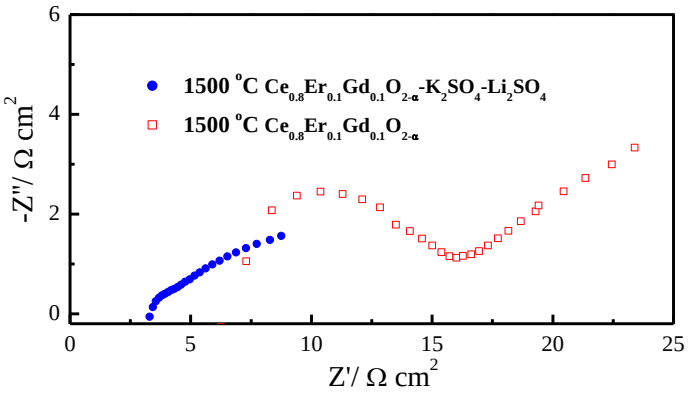

Figure 4. Typical impedance spectra of $Ce_{0.8}Er_{0.1}Gd_{0.1}O_{2-\alpha}$ (1500 °C) and $Ce_{0.8}Er_{0.1}Gd_{0.1}O_{2-\alpha}$- K_2SO_4-Li_2SO_4 (1500 °C) measured at 700 °C under open-circuit conditions.

Fig. 4 is the typical impedance spectra of $Ce_{0.8}Er_{0.1}Gd_{0.1}O_{2-\alpha}$ (1500 °C) and $Ce_{0.8}Er_{0.1}Gd_{0.1}O_{2-\alpha}$-$K_2SO_4$-$Li_2SO_4$ (1500 °C) measured at 700 °C under open-circuit conditions. $Ce_{0.8}Er_{0.1}Gd_{0.1}O_{2-\alpha}$ (1500 °C) spectrum exhibits a semicircle at intermediate to high frequencies and an arc at low frequencies. The high frequency related to the bulk resistance of $Ce_{0.8}Er_{0.1}Gd_{0.1}O_{2-\alpha}$- K_2SO_4-Li_2SO_4 (1500 °C) could not be seen due to the instrumental limitations at the tested temperatures. From low frequency, an arc can be attributed to the resistance between the electrode and the electrolyte [9, 33–34]. The different values of high and low frequencies are the polarization resistance (R_p). It can be seen that R_p of $Ce_{0.8}Er_{0.1}Gd_{0.1}O_{2-\alpha}$ (1500 °C) and $Ce_{0.8}Er_{0.1}Gd_{0.1}O_{2-\alpha}$- K_2SO_4-Li_2SO_4 (1500 °C) are 8.7 $\Omega\cdot cm^2$ and 1.1 $\Omega\cdot cm^2$ at 700 °C, respectively [31-34].

Fig. 5 shows the output performance curves of $Ce_{0.8}Er_{0.1}Gd_{0.1}O_{2-\alpha}$ (1500 °C) and $Ce_{0.8}Er_{0.1}Gd_{0.1}O_{2-\alpha}$-$K_2SO_4$-$Li_2SO_4$ (1500 °C) at 700 °C. The open-circuit voltage of $Ce_{0.8}Er_{0.1}Gd_{0.1}O_{2-\alpha}$ (1500 °C) is low because Ce^{4+} in electrolyte partly reduced to Ce^{3+} under high temperature and an anode reduction atmosphere. Open circuit voltage of $Ce_{0.8}Er_{0.1}Gd_{0.1}O_{2-\alpha}$-$K_2SO_4$-$Li_2SO_4$ (1500 °C) is over 1.05V. This shows that adding a certain amount of sulphate can effectively inhibit the electronic conductivity. The cell output performance of $Ce_{0.8}Er_{0.1}Gd_{0.1}O_{2-\alpha}$- K_2SO_4-Li_2SO_4 (1500 °C) is better than that of $Ce_{0.8}Er_{0.1}Gd_{0.1}O_{2-\alpha}$ (1500 °C). The maximum output power densities of $Ce_{0.8}Er_{0.1}Gd_{0.1}O_{2-\alpha}$ (1500 °C) and $Ce_{0.8}Er_{0.1}Gd_{0.1}O_{2-\alpha}$-$K_2SO_4$-$Li_2SO_4$ (1500 °C) are 16.3 $mW\cdot cm^{-2}$ and 98.1 $mW\cdot cm^{-2}$ at 700 °C, respectively. The good fuel cell performance of $Ce_{0.8}Er_{0.1}Gd_{0.1}O_{2-\alpha}$-$K_2SO_4$-$Li_2SO_4$ (1500 °C) is mainly attributed to the high ionic conductivity in the composite.

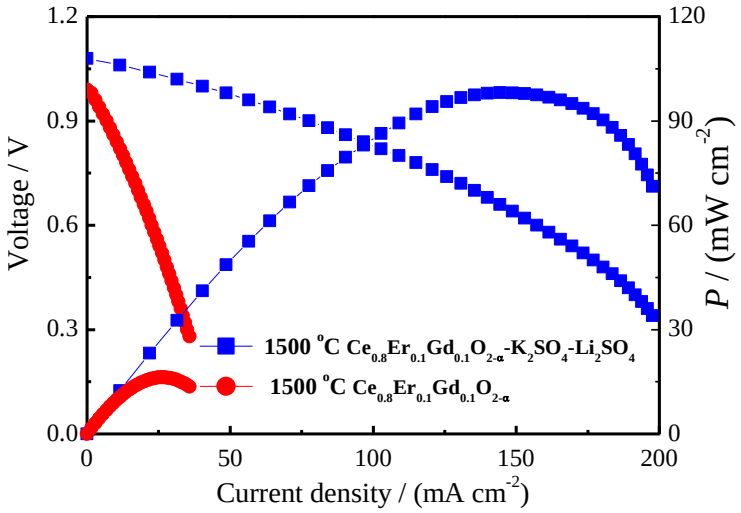

Figure 5. Volt-ampere characteristic curves of $Ce_{0.8}Er_{0.1}Gd_{0.1}O_{2-\alpha}$ (1500 °C) and $Ce_{0.8}Er_{0.1}Gd_{0.1}O_{2-\alpha}$-$K_2SO_4$-$Li_2SO_4$ (1500 °C) at 700 °C.

4. CONCLUSIONS

In this study, Gd^{3+} and Er^{3+} double-doped CeO_2 was mixed with binary sulphates to synthesize $Ce_{0.8}Er_{0.1}Gd_{0.1}O_{2-\alpha}$-$K_2SO_4$-$Li_2SO_4$ composite electrolyte. XRD spectra showed that the $Ce_{0.8}Er_{0.1}Gd_{0.1}O_{2-\alpha}$ structure is not affected by K_2SO_4-Li_2SO_4. The polarization resistance of $Ce_{0.8}Er_{0.1}Gd_{0.1}O_{2-\alpha}$ (1500 °C) and $Ce_{0.8}Er_{0.1}Gd_{0.1}O_{2-\alpha}$- K_2SO_4-Li_2SO_4 (1500 °C) are 8.7 $\Omega \cdot cm^2$ and 1.1 $\Omega \cdot cm^2$ at 700 °C, respectively. The maximum output power densities of $Ce_{0.8}Er_{0.1}Gd_{0.1}O_{2-\alpha}$ and $Ce_{0.8}Er_{0.1}Gd_{0.1}O_{2-\alpha}$-$K_2SO_4$-$Li_2SO_4$ are 16.3 $mW \cdot cm^{-2}$ and 98.1 $mW \cdot cm^{-2}$ at 700 °C, respectively.

ACKNOWLEDGEMENTS
This work was supported by the National Natural Science Foundation (No. 51402052) of China, The Natural Science Project of Anhui Province (No. KJ2019A0539), Horizontal cooperation project of Fuyang municipal government and Fuyang Normal University (No. XDHXTD201704, HX2019004000).

References

1. G. L. Liu, W. Liu, Q. Kou and S. J. Xiao, *Int. J. Electrochem. Sci*., 13 (2018) 2641.
2. T. Hibino, K. Kobayashi, P. Lv, M. Nagao, S. Teranishi and T. Mori, *J. Electrochem. Soc.*, 164 (2017) F557.
3. J. Cao, Y. Ji, X. Huang, H. Jia and W. Liu, *Ceram. Int.*, 44 (2018) 13602.
4. T. Hibino, K. Kobayashi, M. Nagao and S. Teranishi, *ChemElectroChem*, 4 (2017) 3032.
5. Y. Tian, Z. Lü, X. Guo and P. Wu, *Int. J. Electrochem. Sci*., 14 (2019) 1093.
6. C. Bernuy-Lopez, L. Rioja-Monllor, T. Nakamura, S. Ricote, R. O'Hayre, K. Amezawa, M. Einarsrud and T. Grande, *Materials*, 11 (2018) 196.
7. L. Bi, S. Boulfrad and E. Traversa, *Chem. Soc. Rev.*, 43 (2014) 8255.
8. T. Hibino, K. Kobayashi, P. Lv, M. Nagao and S. Teranishi, *Bull. Chem. Soc. Jpn.*, 90 (2017) 1017.
9. 9. J. Luo, A.H. Jensen, N.R. Brooks, J. Sniekers, M. Knipper, D. Aili, Q. Li, B. Vanroy, M. Wübbenhorst, F. Yan, L.V. Meervelt, Z. Shao, J. Fang, Z.-H. Luo, D.E.D. Vos, K. Binnemans and J. Fransaer, *Energy Environ. Sci.*, 8 (2015) 1276.
10. Y. N. Chen, T. Tian, Z. H. Wan, F. Wu, J. T. Tan and M. Pan, *Int. J. Electrochem. Sci.*, 13 (2018)

3827.
11. A.A. Solovyev, S.V. Rabotkin, A.V. Shipilova and I.V. Ionov, *Int. J. Electrochem. Sci*., 14 (2019) 575.
12. J. Li, H. Zhang, M. Gao, Q. Li, W. Bian, T. Tao and H. Zhang, *Materials*, 11 (2018) 749.
13. M. A. Haque, A. B. Sulong, E. H. Majlan, K. S. Loh, T. Husaini and R. Rosli, *Int. J. Electrochem. Sci*., 14 (2019) 371.
14. D.-K. Lim, J.-H. Kim, A.U. Chavan, T.-R. Lee, Y.-S. Yoo and S.-J. Song, *Ceram. Int.*, 42 (2016) 3776.
15. X. Fang, J. Zhu andZ. Lin, *Energies*,11 (2018) 1735.
16. M.S. Arshad, R. Raza, M.A. Ahmad, G. Abbas, A. Ali, A. Rafique, M.K. Ullah, S. Rauf, M.I. Asghar, N. Mushtaq, S. Atiq and S. Naseem, *Ceram. Int.*, 44 (2018) 170.
17. A. Maheshwari and H.-D. Wiemhöfer, *Ceram. Int.*, 41 (2015) 9122.
18. M.R. Kosinski and R.T. Baker, *J. Power Sources*, 196 (2011) 2498.
19. Diaz-Aburto, F. Gracia and M. Colet-Lagrille, *Fuel Cells*, 19 (2019) 147.
20. F. Altaf, R. Batool, R. Gill, G. Abbas, R. Raza, Z. Rehman and M.A. Ahmad, *Ceram. Int.*, 45 (2019) 10330.
21. M. Anwar, Muhammed Ali S.A., A. Muchtar and M.R. Somalu, *Ceram. Int.*, 45 (2019) 5627.
22. M. Kumar, J.-H. Yun, V. Bhatt, B. Singh, J. Kim, J.-S. Kim, B.S. Kim and C.Y. Lee, *Electrochim. Acta*, 284 (2018) 709.
23. S. Kobi, N. Jaiswal, D. Kumar and O. Parkash, *J. Alloy Compd*., 658 (2016) 513.
24. T. Petrisor Jr, A. Meledin, A. Boulle, R.B. Mos, M.S. Gabor, L. Ciontea and T. Petrisor, *Appl. Surf. Sci.*, 433 (2018) 668.
25. B.C. Yang, D. Go, S. Oh, J.W. Shin, H.J. Kim and J. An, *Appl. Surf. Sci.*, 473 (2019) 102.
26. T. Liu, W. Li, Y. Zhang, X. Hao,Y. Zhang, X. Liang, F. Liu, F. Liu, X. Yan, Y. Gao, T. Zhang, C. Zhang and G. Lu, *Sensor. Actuat. B. Chem.*, 284 (2019)751.
27. K.-Y. Park, T.-H. Lee, S. Jo, J. Yang, S.-J. Song, H.-T. Lim, J.H. Kim and J.-Y. Park, *J. Power Sources*., 336(2016) 437.
28. A.I.B. Rondao, S.G. Patricio, F.M.L. Figueiredo and F.M.B. Marques, *Int. J. Hydrogen Energ*., 39(2014) 5460.
29. S. Shawuti and M.A. Gulgun, *J. Power Sources*, 267(2014) 128.
30. B. Zhu, S. Li and B.E. Mellander, *Electrochem. Commun.*, 10 (2008) 302.
31. H. Sun, X. Guo, F. Yu, Z. Yang, G. Li, J. Li, H. Ding, F. Meng, Z. Fan, P. Wang, W. Yan and Z. Hu, *Ceram. Int.*,45 (2019) 7667.
32. J.T. Kim, T.H. Lee, K.Y. Park, Y. Seo, K.B. Kim, S.J. Song, B. Park and J.Y. Park, *J. Power Sources*, 275(2015) 563.
33. G. Zhang, W. Li, W. Huang, Z. Cao, K. Shao, F. Li, C. Tang, C. Li, C. He, Q. Zhang and L. Fan, *J. Power Sources*, 386(2018) 56.
34. Q.X. Fu, S.W. Zha, W. Zhang, D.K. Peng, G.Y. Meng and B. Zhu, *J. Power Sources*,104(2002) 73.
35. C. Slim, L. Baklouti, M. Cassir and A. Ringuedé, *Electrochim. Acta*, 123 (2014) 127.
36. X. Liu, N. Fechler and M. Antonietti, *Chem. Soc. Rev.*, 42 (2013) 8237.
37. S.Phokha, S.Hunpratub, B. Usher, A.Pimsawat, N.Chanlek and S.Maensiri, *Appl. Surf. Sci.*, 446 (2018) 36.
38. S. Preethi, M. Abhiroop and K.S. Babu, *Ceram. Int.*, 45 (2019) 5819.
39. M.A. Rodrigues, A.C. Catto, E. Longo, E.Nossol and R.C. Lima, *J. Rare Earth.*, 36 (2018) 1074.